This project is part of the PRIMA programme supported by the European Union

PRIMA-SECTION 2-2022

"Modelling and Technological Tools to Prevent Surface and Ground-Water Bodies from Agricultural Non-Point Source Pollution Under Mediterranean Conditions"

NPP-SOL

Report on the validation of BR in the Italian and Israeli Case Studies

Deliverable number: D3.1

This project is part of the PRIMA programme supported by the European Union

Non-Point Pollution SOLutions (NPP-SOL)

Deliverable number: D3.1

Report on the validation of BR in the Italian and Israeli Case Studies

Authors	Antonio Coppola (University of Cagliari) Alessandro Comegna (University of Basilicata) Shawkat B. M. Hassan (University of Cagliari) Roy Posmanik (Technion – Israel Institute of Technology) Roey Egozi (Ministry of Agriculture and Food Security) Elazar Volk (Ministry of Agriculture and Food Security) Paolo Botti (Regional Agency for the Sardinia River Basin District) Mario Lorrai (Regional Agency for the Sardinia River Basin District) Massimo Gaetano Aiello (Regional Agency for the Sardinia River Basin District)
Approved by reviewers	Albert Soler Gil (University of Barcelona)
Date of approval	23/10/2026
Approved by project coordinator	Antonio Coppola (University of Cagliari)
Date of approval	23/10/2026
Call	PRIMA Section 2 2022 – Multi-topic Topic 2.1.1 RIA Prevent and reduce land and water salinization and pollution due to agri-food activities
Project URL	https://npp-sol.iamm.ciheam.org/

NPP-SOL Non-Point Pollution Solutions
PRIMA PARTNERSHIP FOR RESEARCH AND INNOVATION IN THE MEDITERRANEAN AREA
This project is part of the PRIMA programme supported by the European Union

Abstract

Woodchip bioreactors (BRs) were evaluated in the Italian and Israeli NPP-SOL case studies to assess their operation and nitrogen-removal performance under Mediterranean agricultural conditions. The Italian case study follows the initial drainage-coefficient design, a site-specific update using coupled FLOWS–KWV simulations, and field hydraulic and nitrate-removal testing. The initial design specified a treatment flow of approximately 4.45 L s^{-1} and a target contact time of 4–5 h. The updated calculation for a 9 ha pilot field gave a maximum required saturated woodchip volume of 61.8 m^3. Five quasi-steady hydraulic windows covered mean flows of 70.2–259.5 m^3 d^{-1} and showed a stage-dependent apparent saturated hydraulic conductivity. Nitrate attenuation under favourable loading gave way to breakthrough under strong hydraulic forcing, while carbon chemistry and low dissolved oxygen supported a reactive woodchip bed. The association between apparent hydraulic conductivity and estimated flow section is compatible with uneven bed use, but effective residence time and preferential flow require independent tracer verification.

The Israeli reactor at Newe Ya'ar Research Center was assessed during rainfall/runoff events and dry-season treated-wastewater operation. Continuous monitoring was combined with internal, depth-resolved and inlet–outlet sampling. Mean total nitrogen decreased from approximately 6 to 3 mg N L^{-1}, corresponding to about 50% concentration reduction. A preliminary headspace campaign detected dissolved N_2O at the inlet but not at the middle or outlet, while NH_3 decreased along the treatment path. These measurements describe aqueous nitrogen species and do not quantify emission fluxes.

Together, the studies demonstrate nitrogen attenuation in operating BRs and show that hydraulic history, carbon availability and seasonal water supply must be considered when interpreting performance. Completed tracer analysis and transport-aligned flow and chemistry measurements are needed to establish effective residence time and nitrogen mass balances.

1. Introduction

Agricultural drainage and runoff transfer nutrients (nitrate, phosphorus,…) and other agrochemicals from cultivated soils to shallow groundwater and surface-water networks. Nitrate represents one of the main problems in areas with intensive livestock activities. Farm-scale woodchip bioreactors (BR) offer a practical means of intercepting nitrate-rich water close to its source and treating it before discharge to receiving waters.

BR woodchips provide carbon and surfaces for microbial growth. Under oxygen-limited conditions, microorganisms use carbon to support heterotrophic denitrification, reducing nitrate through intermediate nitrogen species to gaseous nitrogen. The performance of a BR consequently depends on the interaction between water movement and microbial reaction conditions, including temperature, nitrate supply and the availability of biodegradable carbon (Schipper et al., 2010; Hoover et al., 2016). Increasing residence time generally increases treatment opportunity, although excessive reduction can favour secondary processes. This makes designing a BR in Mediterranean farming systems quite challenging because of rainfall seasonality and intensive irrigation, inducing alternating periods of high drainage, low flow and limited water availability, which makes the pollutant load entering a treatment system and the time available for removal very variable in time.

The NPP-SOL design deliverable D2.1 established the drainage-interception concept, the construction of the reactive beds, the inlet and outlet control structures, and the monitoring and tracer methods required to assess their functioning (Coppola et al., Report on designing Drainage System and BR Deliverable number: D.2.1). Field validation addresses the next step: whether the installed systems provide effective treatment under their actual hydraulic and seasonal conditions. Actually, nominal BR dimensions and pore volume coming from the designing phase, define a theoretical contact time, but they do not describe the real variability of residence-time of water passing through the BR bed due to the fluctuations of water and nitrate loadings.

In addition to the time variability of flow conditions inside the BR, in woodchip media, flow resistance can depart from Darcy behaviour and internal flow paths may use the reactive volume unevenly (Ghane et al., 2014). In fact, high-frequency monitoring in BR has shown that nitrate peaks can arrive at the outlet well after they occur at the inlet, which may suggest preferential flow paths inside the BR. As variability in storage and transport along the BR also affect paired inlet–outlet chemistry, this may well lead to misleading instantaneous removal estimates (Maxwell et al., 2020).

The present deliverable reports validation in two complementary settings. The Italian case study uses controlled hydraulic changes and chemical measurements to examine the functioning of one of the four pilot farms' bioreactors in Arborea, Sardinia, Italy. The Israeli case study follows construction and adaptation of the Newe Ya'ar reactor, monitoring during wet and dry periods, nitrogen attenuation along the treatment path and investigation of possible gaseous nitrogen trade-offs. The Italian results concern nitrate expressed as NO_3^-, whereas the Israeli principal indicator is total nitrogen expressed as N. Their findings are therefore presented separately, following the experimental approach and interpretation appropriate to each system.

2. Validation of the Italian case study

2.1. Initial design

The Italian case study area is the Arborea plain, Sardinia. A subsurface drainage system was designed and installed to intercept nitrate-rich agricultural drainage before discharge to the surrounding surface drainage network. The subsurface drainage system conveys the agricultural drainage to an edge-of-the-field treatment technology (woodchip bioreactor).

The initial design is detailed in deliverable D2.1. The drainage layout followed the regular field geometry: parallel perforated laterals ran along the long side of the fields and discharged into a collector along the short side. A preliminary three-year groundwater record showed a shallow water table around 0.90–1.10 m below the soil surface. Drains were therefore placed at approximately 1.00 m depth, with 20 m spacing determined using the Hooghoudt approach and measured soil hydraulic properties. This position was intended to intercept percolating water and nitrate as recharge raised the water table above the drain level. DN90 laterals were specified, with a design slope of 1‰, and collector diameters of DN250 were selected.

Sizing initially used a drainage coefficient of 12 mm d^{-1} and a representative contributing area of 16 ha. Their product gave a theoretical peak drainage flow of 1,920 m^3 d^{-1}. The reactor was sized to treat 20% of that peak, or 384 m^3 d^{-1}, equivalent to approximately 4.45 L s^{-1}. Excess drainage was diverted through a bypass. The target retention time was approximately 4–5 h, providing the initial basis for a trench 25 m long, 4 m wide and 1.20 m deep lined trench. These were design assumptions for the original farm-scale installations, rather than measurements of the residence time subsequently achieved during actual operation. Table 1 summarizes the main specifications for the drainage system and BR in the Italian CS in the initial design as described in deliverable D2.1.

Table 1. Main parameters of the initial Arborea drainage and BR design (Deliverable D2.1).

Parameter	Initial design value
Drain depth and spacing	1.00 m and 20 m
Treatment flow	384 m^3 d^{-1}, approximately 4.45 L s^{-1}
Target retention time	Approximately 4–5 h
Trench dimensions	25 m × 4 m × 1.20 m
Reactive medium and cover	0.90 m eucalyptus woodchips; 0.30 m soil cover
Lining and hydraulic control	2 mm HDPE liner with protective geotextile; inlet pump, bypass and adjustable outlet weir

The bottom and walls were lined with a 2 mm HDPE waterproof membrane, protected by geotextile, to limit leakage to the subsoil. Locally available eucalyptus woodchips filled the lower 0.85 m, with a separating geotextile beneath a 0.30 m soil cover. The inlet structure was installed with three chambers: the first received drainage and housed the submersible pump, the second supplied the reactor (i.e., the woodchip-filled trench) and the third conveyed overflow to the bypass (Figure 1). A transverse perforated PVC diffuser distributed inflow across the trench bed width. A similar pipe collected treated water at the downstream end.

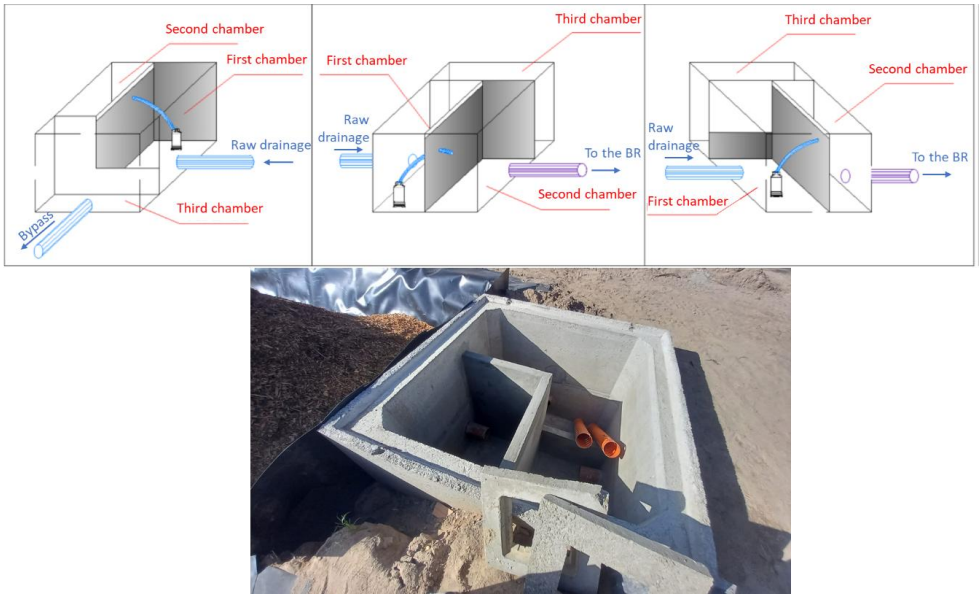


Figure 1. The three-chamber inlet structure, showing collection of drainage, pumping towards the BR and excess-flow bypass, together with the constructed inlet manhole (Coppola et al., n.d.).

The two-chamber outlet structure received the treated water and maintained the downstream level through a weir with modular gates. Changing the gate height adjusted the head difference across the woodchips and provided a means of controlling velocity as the hydraulic properties of the medium changed. Check valves on the bypass and treated-water discharge prevented channel water from returning to the reactor. Inlet and outlet multiparameter probes, internal piezometers, periodic water sampling and woodchip inspection points were included to verify hydraulic conditions, nitrate attenuation and medium condition during operation.

2.2. Refined BR design

The design was subsequently refined for a 9-ha pilot field by replacing the single drainage-coefficient estimate with daily predictions of the water and nitrate delivered to the BR. The updated approach coupled the agrohydrological model FLOWS (Coppola et al., 2025; 2026a,b) with the drainage-routing model KWV (Coppola et al., 2024). FLOWS calculated water flow, nutrient transformations and nitrate transport in the soil, including water and nitrate fluxes into the lateral drains. KWV then routed water and nitrate fluxes, using the kinematic wave and the Advection-Dispersion Equation (ADE), respectively, along the laterals and collectors to obtain the inlet discharge hydrograph and associated nitrate concentrations. The sequence linked reactor sizing to the actual field, cropping system, irrigation, fertilisation and groundwater conditions (Figure 2). The approach and the results are detailed in Hassan et al. (2026)

The pilot field was cultivated with corn in summer and ryegrass in winter. Its two sandy horizons contained more than 90% sand; measured saturated hydraulic conductivities used in the simulations were 300 cm d^{-1} for the upper horizon and 50 cm d^{-1} for the underlying horizon. The installed drainage network retained the 1 m drain depth and 20 m spacing. In this site-specific layout, lateral diameter was 0.08 m and collector diameter was 0.20 m, with a common pipe slope of 3 mm/m, which was different from the initial design of 1 mm/m. Two collector branches, approximately 170 m and 90 m long, conveyed drainage to the BR on the northern field boundary, as shown in figure 3. These network dimensions were used in the updated calculation.

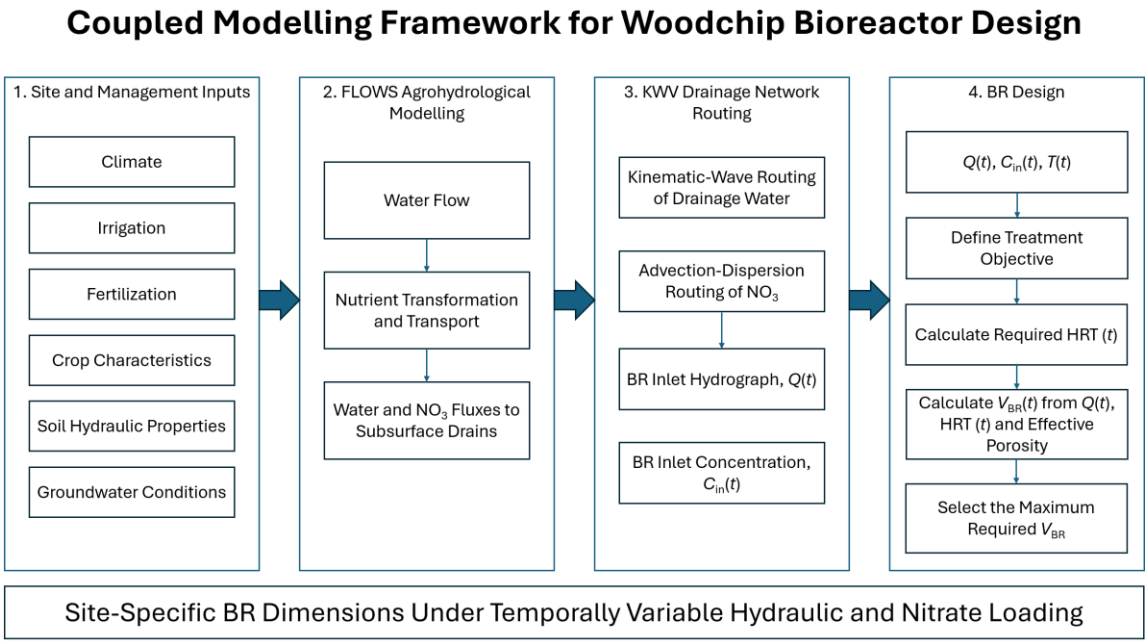


Figure 2. Updated design sequence linking site information, FLOWS soil and drainage simulations, KWV routing and BR sizing from time-varying inlet discharge, nitrate concentration and temperature.



Figure 3. Layout of the drainage system and the BR position in the pilot area in the Italian case study. The drainage pipes are represented in celeste lines and the black lines are the field borders.

The simulations covered 1 June 2024–1 June 2025 and distinguished summer and winter groundwater conditions. Regional groundwater depth was around 1.00 m in summer and 0.80 m in winter, with groundwater nitrate concentrations of 500 and 300 mg NO_3^- L^{-1}, respectively. Rainfall, sprinkler irrigation and the urea, mineral fertiliser and manure application data were collected and used as inputs for FLOWS simulations. Water exchange with the regional aquifer was represented within the soil profile, alongside drainage extraction. This approach was necessary because the shallow regional groundwater supplied/received both water and nitrate to/from the soil profile.

Predicted inlet conditions were compared with discharge monitoring and laboratory nitrate analyses collected during the same year. Simulated summer and winter peak discharges were 116 and 230 m^3 d^{-1}, compared with measured peaks of 104 and 245 m^3 d^{-1}. Simulated peak nitrate concentrations were 493 mg NO_3^- L^{-1} in summer and 320 mg NO_3^- L^{-1} in winter, compared with measured peaks of 500 and 366 mg NO_3^- L^{-1} (Table 2). The simulations reproduced the seasonal peak conditions but smoothed part of the observed short-term variability, consistent with the use of fixed seasonal regional groundwater levels and concentrations.

Table 2. Simulated and measured seasonal peak discharges and concentrations at the BR inlet during 1 June 2024–1 June 2025. Peaks in different variables need not occur on the same day.

Inlet variable	Summer	Winter
Simulated peak discharge ($m^3\ d^{-1}$)	116	230
Measured peak discharge ($m^3\ d^{-1}$)	104	245
Simulated peak nitrate (mg $NO_3^-\ L^{-1}$)	493	320
Measured peak nitrate (mg $NO_3^-\ L^{-1}$)	500	366

Although summer inlet concentrations were higher, the largest predicted nitrate loading (nitrate mass flues) occurred in winter, between November and January, reaching approximately 74 kg $NO_3^-\ d^{-1}$. The higher winter water table generated larger drainage flows, which outweighed the seasonal reduction in concentration. The updated sizing therefore evaluated each day's combination of discharge, nitrate concentration and temperature, rather than assuming that the day with the highest concentration governed the reactor size.

The treatment target was an outlet concentration of 50 mg $NO_3^-\ L^{-1}$, equivalent to approximately 11.3 mg N L^{-1}. Required contact time was calculated using temperature-adjusted Michaelis–Menten nitrate-removal kinetics following the modelling approach of Ghane et al. (2015). The required saturated woodchip volume was then obtained from discharge, required contact time and an effective porosity of 0.45. With Q in $m^3\ d^{-1}$ and required contact time τ in hours, the sizing relationship is:

$$V_{\mathrm{BR}} = \frac{Q\tau}{24 n_{\mathrm{e}}} \quad (1)$$

Here V_{BR} is the bulk saturated woodchip volume and n_e is the effective porosity; the corresponding pore-water volume is ($n_e\ V_{BR}$). The maximum required woodchip volume reported for the simulated year was 61.8 m^3, with a required contact time of 3.86 h under the critical winter conditions. A summer value of 3.57 h was obtained on 2 June 2024, but the lower summer discharge required a smaller reactor volume. The updated calculation thus checked the combination of flow, concentration and temperature throughout the year.

The available strip between the cultivated field and a tree line constrained the updated BR width to 3 m. An average wetted depth of 0.85 m gave a design cross-section of 2.55 m^2. Dividing 61.8 m^3 by that section gives a calculated design length of approximately 24.2 m, which was rounded up to 25 m.

The updated hydraulic arrangement retained a three-chamber inlet, excess-flow bypass, transverse diffusers and a two-chamber outlet with an adjustable downstream level. It also incorporated a backwash arrangement (Figure 4). A temporary pipe allowed the inlet pump to deliver water to the outlet structure, while a temporary pump at the inlet discharged water to the drainage channel. Reversing the hydraulic gradient in this way allowed water to flow through the woodchip bed from the outlet to the inlet structure. A flowmeter, inlet and outlet water-level sensors, multiparameter probes and periodic laboratory analyses provided the measurements needed to analyze the BR performance and to validate the design framework.

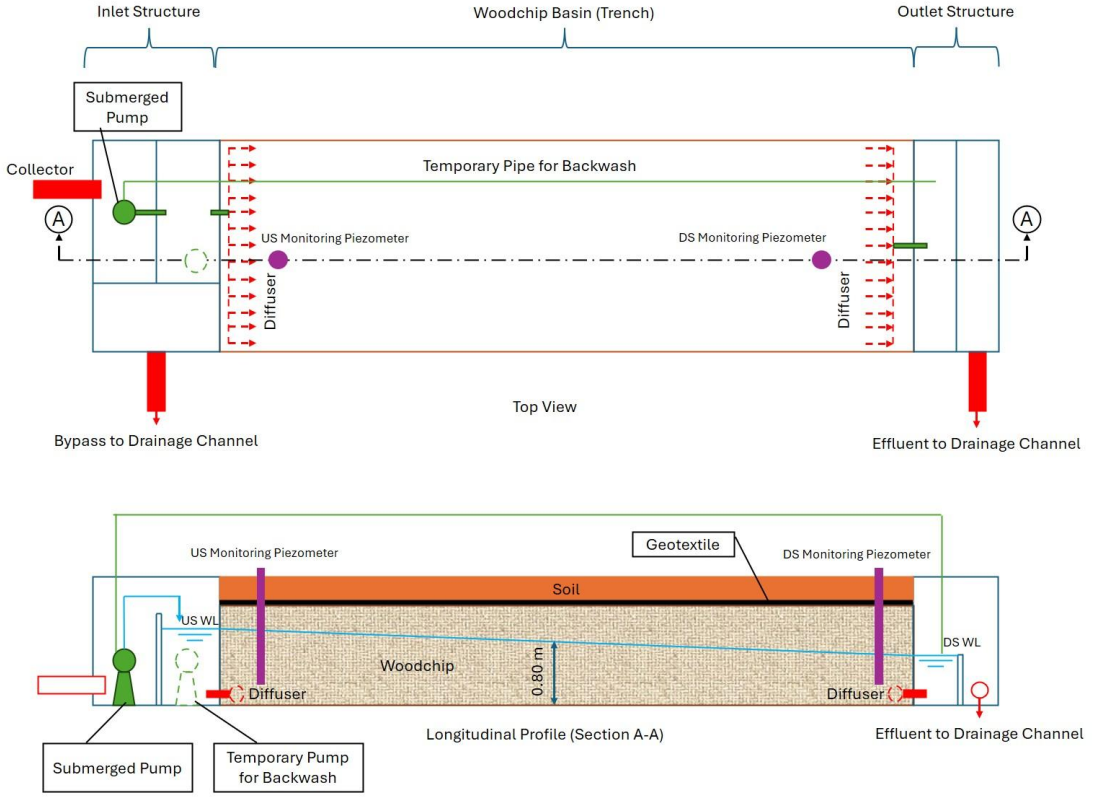


Figure 4. Updated BR layout with inlet pumping and bypass, woodchip trench, monitoring piezometers, transverse diffusers, controlled outlet and temporary backwash connections. The drawing shows an indicative 0.80 m water depth; the sizing calculation uses a mean wetted depth of 0.85 m.

2.3. BR hydraulic performance

Field verification deliberately imposed changes in flow to test how the constructed BR responded to different hydraulic loads. The time series of inlet and outlet levels and total drainage flow indicate that the bioreactor was subjected to different hydraulic regimes during the stress tests. Although transient conditions dominate most of the record, several intervals exhibit sufficiently stable water levels and flow rates to support the use of Darcy's law as an approximate diagnostic tool. For these intervals, the Darcy-based value provides a reasonable estimate of the saturated hydraulic conductivity or, more cautiously, an equivalent steady-state hydraulic measure derived from the flow rate, estimated flow cross-sectional area, and hydraulic gradient. This is why we opted to cautiously call the saturated hydraulic conductivity coming from this analysis as apparent saturated hydraulic conductivity, Kapp.

The corrected inlet level, outlet level and drainage-flow record shows filling, rapid increases in inflow, sustained high-flow plateaus, interruptions and recessions (Figure 5). The inlet level changed more strongly than the outlet level, which was constrained by the downstream control structure. During filling and recession, the difference between inflow and outflow changes the water stored in the bed; these periods cannot be treated as uniform steady flow through a fixed reactive volume.

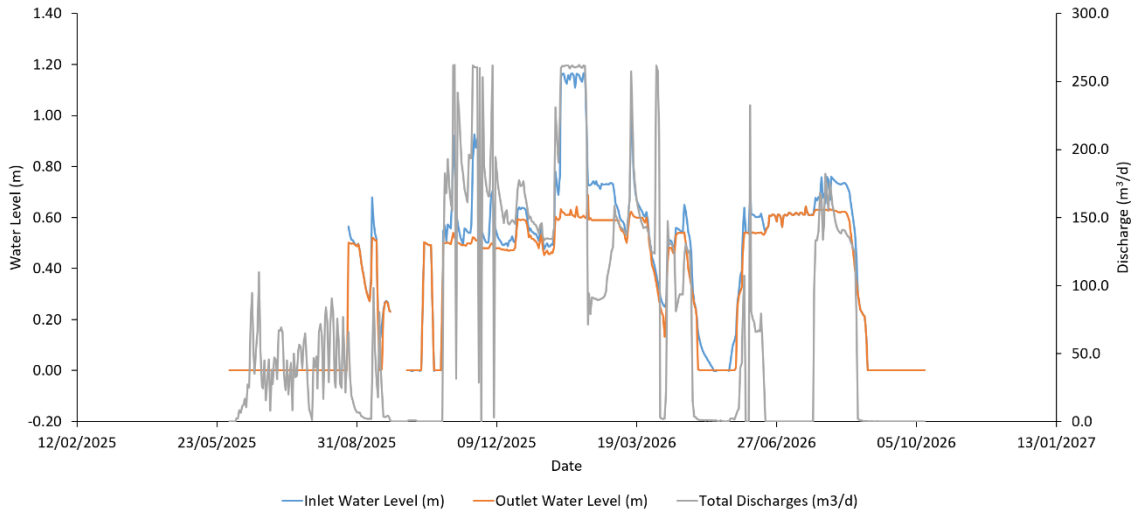


Figure 5. Corrected inlet level (blue), outlet level (orange) and drainage discharge (grey) during the imposed hydraulic stress test. Levels use the left axis in metres and discharge the right axis in m³ d⁻¹.

Five quasi-steady windows were identified by examining both the level–flow record and within-period variability (Table 3 and figure 6). The selection required several consecutive days of non-zero flow, limited changes in water levels, a positive hydraulic gradient and a consistent apparent conductivity. The diagnostic calculation used the estimated flow cross-sectional area A_w and the head gradient i:

$$i = \frac{h_{\text{in,corr}} - h_{\text{out}}}{L} \qquad K_{\text{app}} = \frac{Q}{A_w i} \tag{2}$$

Where Q in m³ d⁻¹ and A_w in m², K_{app} is expressed in m d⁻¹.

Table 3. Quasi-steady hydraulic windows identified during the stress test. All dates are in 2026; n is the number of daily observations. A_w denotes the estimated flow cross-sectional area used in the diagnostic calculation. Kapp is the median of the values in each of the quasi steady-state interval

ID	Period	n	Mean Q (m³ d⁻¹)	Mean A_w (m²)	Mean i (–)	Median K_{app} (m d⁻¹)
P1	24 Jan–11 Feb	19	259.5	0.732	0.0212	16,459
P2	13–20 Feb	8	89.3	0.552	0.0056	28,978
P3	22 Feb–2 Mar	9	106.2	0.550	0.0056	33,947
P4	9–17 Jun	9	70.2	0.444	0.0026	59,619
P5	6–22 Aug	17	139.3	0.401	0.0046	74,755

The gradient calculation used the 25 m reactor length. The Table 3 shows that the BR flow cross section, A_w, changes over time to the fluctuating water load coming from the drainage network. and the corresponding values are distinct from the fixed 2.55 m² cross-section used in the updated sizing calculation. Also, the K_{app} in the table (calculated as the median of the values in each of the quasi steady-state interval, depend on the area estimate and the common reference used for the two water levels and cannot be identified as a single hydraulic characteristic of the BR independent on the flow

conditions. By contrast, it would suggest the presence of different woodchip layers, each with a different conductivity value, inducing a different Kapp value depending on the height of the BR cross section actually involved in the flow.

P1, from 24 January to 11 February, was the clearest high-flow plateau. Mean discharge was 259.5 m^3 d^{-1} and its coefficient of variation was only 2.7%. Mean corrected inlet and outlet levels were 1.142 and 0.611 m, giving a head difference of approximately 0.531 m and a gradient of 0.0212. Median Kapp was 16,459 m d^{-1}, with a coefficient of variation of 10.1%. The relatively large head difference reduced sensitivity to small level errors, although high-flow resistance in woodchips may depart from Darcy behaviour (Ghane et al., 2014).

Following the transition on 12 February, P2 and P3 operated at lower flows of 89.3 and 106.2 m^3 d^{-1}. Mean inlet and outlet levels were approximately 0.73 and 0.59 m in both periods, and the mean gradient was about 0.0056. Their median Kapp values were 28,978 and 33,947 m d^{-1}. Flow coefficients of variation were 5.0% and 14.0%, respectively. These windows show that a comparatively stable level difference could accompany different discharges and apparent conductivities.

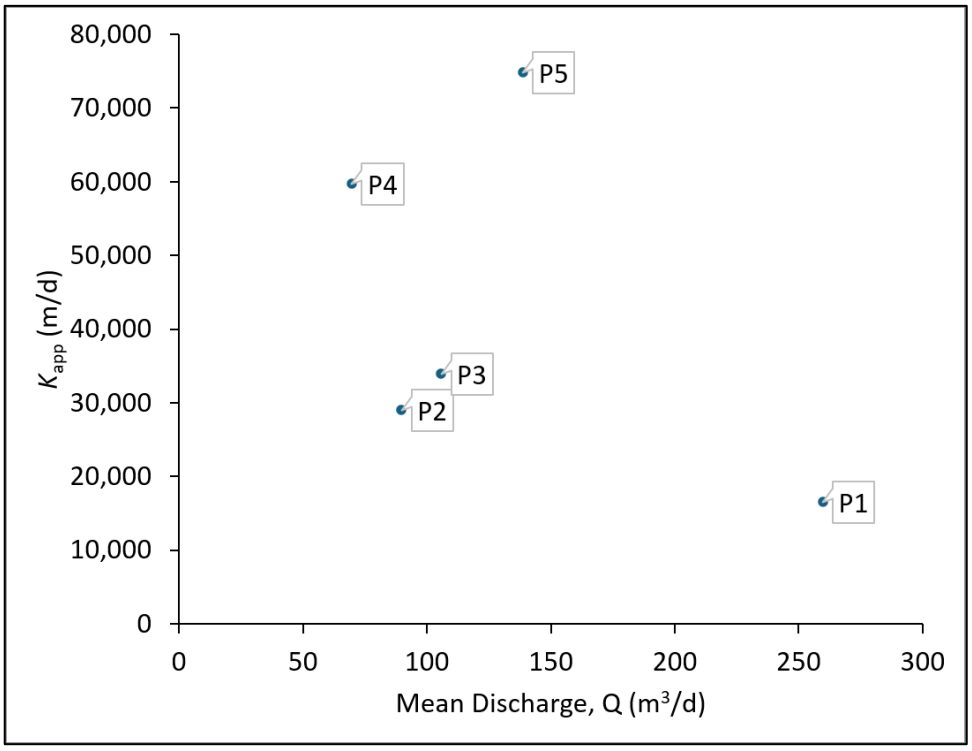


Figure 6. Median apparent Darcy-based conductivity against mean discharge for the five quasi-steady windows. The values depend on the stage-specific flow sections and gradients used in the calculation.

P4 followed the interruptions and flow pulse of 4–8 June. Between 9 and 17 June, mean flow was 70.2 m^3 d^{-1} and median Kapp was 59,619 m d^{-1}, with only 1.0% within-period variation in Kapp. Nevertheless, the mean gradient was small, 0.0026, so millimetric uncertainty in the water levels could appreciably change the result. P5, from 6 to 22 August, was a smooth recession rather than a constant-head plateau. Mean discharge was 139.3 m^3 d^{-1} and median Kapp was 74,755 m d^{-1}, with 2.0% variation, while levels and the estimated flow section progressively decreased. Its stable ratio of Q to Aw i describes a coherent recession response.

K_{app} did not increase monotonically with discharge: the largest flow in P1 produced the lowest apparent conductivity (Figure 6). The relationship with estimated flow cross section was clearer, with the largest values occurring at the smallest sections (Figure 7). One possible explanation is that low Aw concentrate conveyance in a relatively conductive basal part of the bed. As water level rises, additional woodchip zones may become saturated but contribute less flow per unit area because of greater tortuosity or weaker connection to the outlet. Under this interpretation, raising the water level could recruit more reactive volume and reduce the relative contribution of a fast basal pathway.

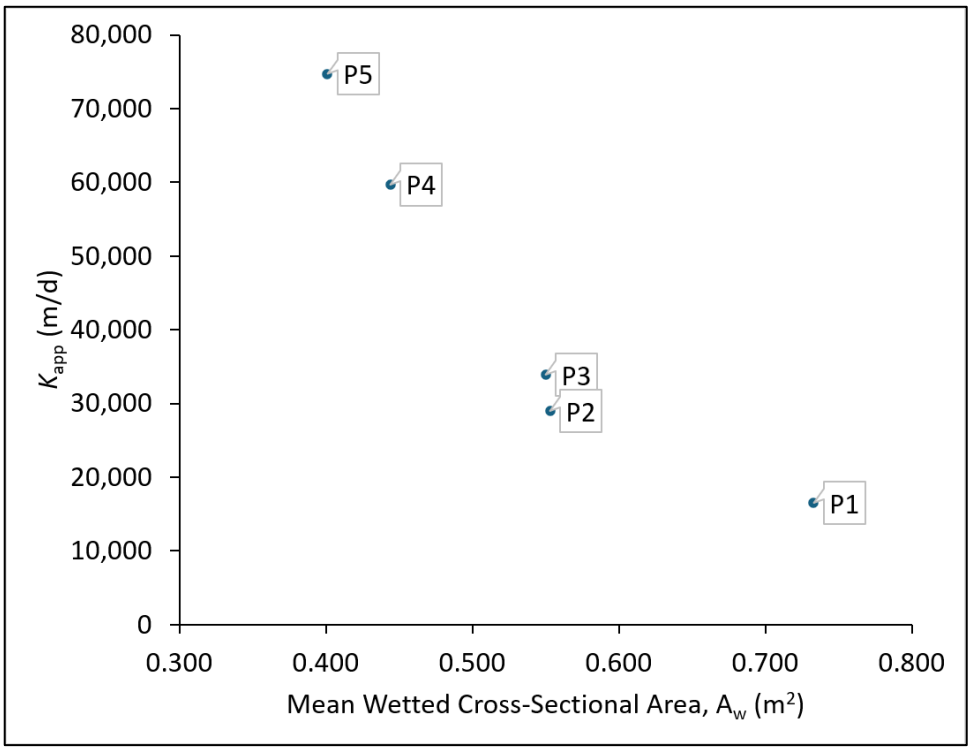


Figure 7. Median apparent Darcy-based conductivity against the estimated flow section. The inverse pattern is compatible with stage-dependent use of the bed but is not independent proof of preferential basal flow.

The area–conductivity relationship alone cannot establish that mechanism, because Aw is also in the denominator of the Kapp calculation. Uncertainty in section, small head differences, outlet control and transient storage can generate similar patterns. A sodium-bromide tracer test, using a NaBr solution at 50 g L^{-1}, has been planned to determine the residence-time distribution independently. Early arrival, a sharp peak and a long tail would support non-uniform transport; the mean travel time, recovery and effective pore volume are needed to test how much of the bed participates in treatment. Breakthrough results were not yet available in the performance assessment, so the approximately 5 h nominal contact time remains a reference to be tested.

2.4. BR nitrate removal performance

Figure 8 illustrates the BR monitoring data in terms of the hydraulic loading, nitrate inlet and outlet concentrations, as well as the daily treated nitrate masses. The inlet–outlet chemistry showed two contrasting responses during the hydraulic stress test. During the earlier phases, and under low or moderate hydraulic loading, outlet concentrations were significantly lower than inlet concentrations. During or following increased flow, outlet nitrate rose towards the inlet concentration. This

breakthrough occurred even when the inlet concentration was not at its maximum, indicating that the increased hydraulic load could significantly limit treatment by reducing the time available for contact with the woodchips. Flow variation was deliberately imposed to reveal this transition, rather than being treated as an unexplained interruption of normal operation. In any case, the BR efficiency changes non-linearly with the discharge and suggest a quite complex denitrification chemical-microbial response to the hydraulic conditions. This could also be connected to the changes of K_{app} associated with the flow regime. In this sense, the BR bio-geochemical performance should be evaluated by accounting for the specific layer of the woodchip bed involved in the flux inside the BR.

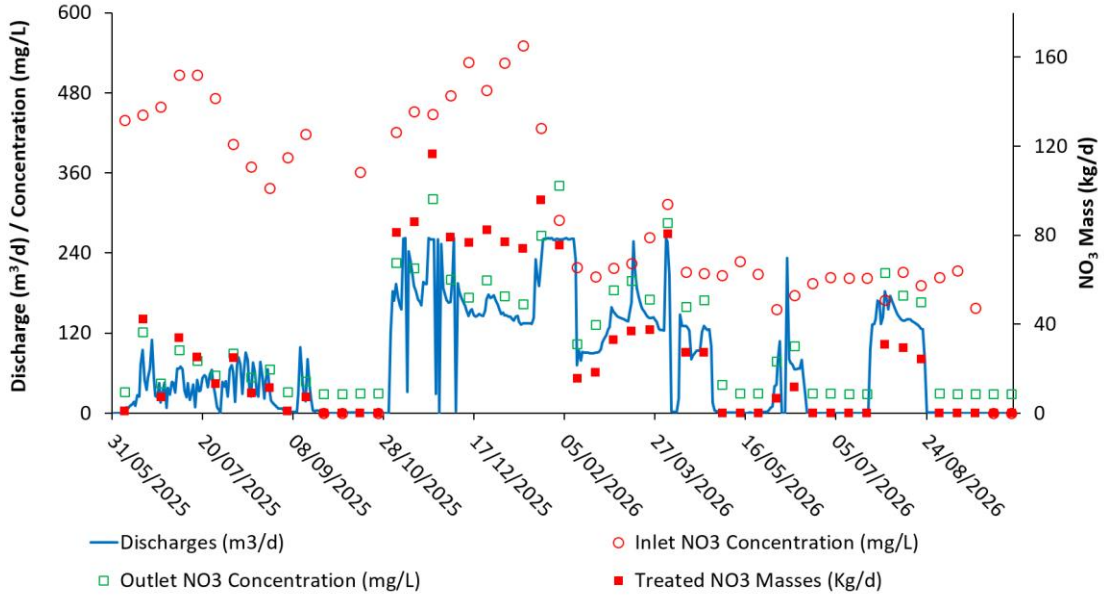


Figure 8. The BR monitoring data in the Italian case study. The hollow red circles represent the measured inlet nitrate concentrations. The hollow green squares represent the measured outlet nitrate concentrations. The blue line represents the daily discharges through the BR. The solid red squares represent the treated daily nitrate masses.

However, the BR nitrate removal performance should not be evaluated based only on concentration attenuation; nitrate mass removal should also be accounted for. During the earlier phases, which were characterized by low hydraulic loads and high concentration attenuation, the nitrate mass removal was lower compared to the following phases where the hydraulic loads were higher and the concentrations attenuation were lower. Since the nitrate concentrations were measured once every 10 days, the entire set of daily nitrate mass removal values for the entire monitoring period were interpolated from the measured values (the ones taken every 10 days). The cumulative nitrate mass removed by the BR was, thus, estimated at 14014 kg, corresponding to 3153 kg of N-NO_3.

The January–February high-flow plateau provides a specific example. During P1, when mean drainage flow was around 260 m^3 d^{-1}, outlet nitrate was comparable to, and at times greater than, the inlet concentration. Stable discharge and water levels therefore did not imply chemical steady state. The outlet could contain nitrate-rich water admitted earlier or mobilised from storage as the flow increased. A same-day outlet concentration above the inlet consequently does not by itself demonstrate nitrate production within the reactor. The inlet history and transport lag must be considered, as shown for other field woodchip systems by Maxwell et al. (2020).

Performance was evaluated using both concentration attenuation and the nitrate load associated with the treatment flow. Concentration removal describes the relative inlet–outlet difference, whereas the load difference expresses the nitrate flux associated with that difference at the prevailing discharge:

$$\eta_C = 100\,\frac{C_{in} - C_{out}}{C_{in}}$$
$$\Delta L_{NO_3} = \frac{Q(C_{in} - C_{out})}{1000} \quad (3)$$

Here η_C is the nitrate concentration attenuation in percent. When Q is in $m^3\ d^{-1}$ and concentrations are in mg $NO_3^-\ L^{-1}$, ΔL_{NO3} is the nitrate mass removal in kg $NO_3^-\ d^{-1}$. Nitrate-ion mass is converted to nitrogen mass by multiplying by 0.225. A high percentage reduction at very low flow can correspond to a small, treated mass, whereas a lower percentage at a high flow can still correspond to a substantial nitrate-load difference. The load calculation assumes that Q represents the flow passing through the reactive bed. During storage changes, separate inlet and outlet flows and transport-aligned concentrations are needed for a closed balance; bypassed drainage must also be included when assessing the whole drainage system.

Supporting chemistry indicated that the woodchips remained reactive. Dissolved oxygen was generally low during the efficient phases, while outlet total organic carbon (TOC) was often higher than inlet TOC, particularly early in monitoring. The TOC increase is consistent with carbon release from the woodchips, providing an electron donor for heterotrophic denitrification. Outlet increases in total inorganic carbon (TIC) and alkalinity also accompanied nitrate attenuation, consistent with microbial carbon oxidation and changes in the carbonate system. These observations support denitrification as the main interpretation of nitrate attenuation, while total TOC alone does not quantify the readily biodegradable fraction (Schipper et al., 2010; Hoover et al., 2016).

Outlet nitrite was generally low, so nitrate reduction did not systematically stop at the first intermediate stage. Ammonium was also generally low, with occasional outlet increases that may reflect mineralisation or more strongly reducing microsites. These signals do not establish ammonium production as the dominant nitrate-removal pathway. Sulphate was lower at the outlet on several sampling dates, which is compatible with secondary sulphate reduction where nitrate became locally depleted. Mixing and differences in water age are alternative explanations, and the sulphate response does not establish the extent of that process.

Electrical conductivity and chloride provided complementary information on mixing and storage because their response was more conservative than that of nitrate. The persistence of low oxygen and available organic carbon during high-flow breakthrough suggests a hydraulic limitation, although carbon bioavailability and temperature can also affect the reaction rate. The field response therefore supports an operating strategy that maintains sufficient saturated reactive volume and contact time as flow increases, using the inlet control, outlet level and bypass already provided by the design. It does not justify a single numerical flow threshold or a measured residence time from the present chemistry alone.

The stress test demonstrated nitrate attenuation under favourable loading and breakthrough under strong hydraulic forcing, while the water-level and apparent-conductivity analysis identified changes in the way the bed conveyed water. The bromide test is needed to determine whether high-flow breakthrough reflects a broadly shortened residence time, preferential basal flow, exchange with stored water or a combination of these mechanisms. Relating its residence-time distribution to the monitored flows and chemistry will allow the nominal design conditions to be tested against the actual reactive flow volume.

3. Validation of the Israeli case study

3.1. Site, objective and bioreactor design

The Israeli NPP-SOL case study is located at the Model Farm for Sustainable Agriculture, Newe Ya'ar Research Center, in the Jezre'el Valley. The site has a Mediterranean climate, with approximately 570 mm annual rainfall concentrated mainly between November and March. The denitrifying bioreactor (BR) was established as a field-scale treatment unit to reduce nitrogen (N) loads transported by agricultural drainage and runoff before discharge toward the Nahalal Stream.

The BR is approximately 12 m long and 3 m wide (figure 9). Apple-wood chips provide the reactive carbon medium, with gravel layers above and geotextile/polyethylene protection below. The design includes inlet and outlet points and three internal monitoring cross-sections (B, C and D), with sampling at several depths. This layout allows treatment performance to be evaluated not only between inlet and outlet, but also along the flow path and through the reactor profile.

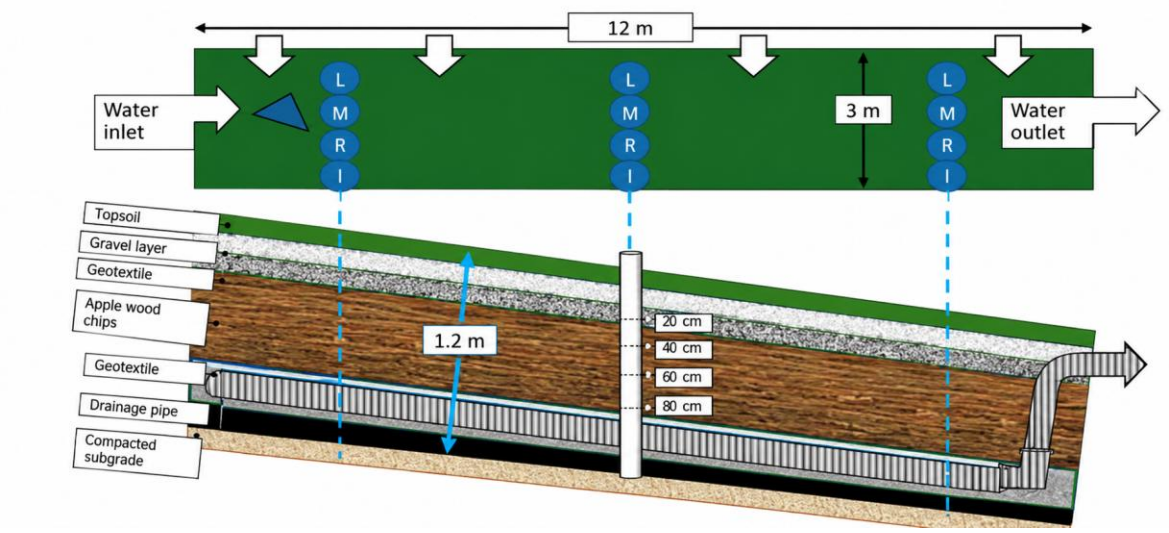


Figure 9. Israeli BR design and monitoring layout. The three internal cross-sections and depth-resolved sampling points were used to follow changes within the reactive zone.

3.2. Construction and adaptation to field conditions

The BR was constructed in December 2023 (figure 10). An extreme storm in January 2024 caused erosion damage, requiring modification and reinforcement of the system in March 2024. The first controlled experiment with treated wastewater was subsequently conducted in June 2024. This sequence was an important part of the field validation, because it demonstrated the need to adapt the original installation to actual hydrological and erosion conditions at the agricultural site. Figure 9 also illustrates the transition from construction to operational testing. During the dry Mediterranean season, treated wastewater was used as supplemental water to compensate for the absence of rainfall and help maintain the saturated, oxygen-limited conditions required for denitrification.



Figure 10. Development of the Israeli BR from construction to controlled operation. The photographs document construction, storm-related erosion, the modified reactor and the first treated-wastewater experiment.

3.3. Monitoring and validation approach

Validation combined continuous environmental monitoring with event-based grab sampling. Sensors and wireless data logging were deployed in and around the BR, while discrete samples were collected during rainfall/runoff events and during dry-season treated-wastewater operation. The monitoring program included inlet and outlet samples together with internal cross-sections and depth-resolved samples. In an intensive campaign, the full configuration yielded up to 36 BR water samples. As shown in figure 11, the combination of continuous measurements and discrete sampling was designed to capture the strongly event-driven behavior of the site. In the second term dataset, 22 BR sampling events were reported: 14 during the wet period and 8 during the dry period. Samples were measured for pH and EC and preserved for additional geochemical analyses at the Technion.

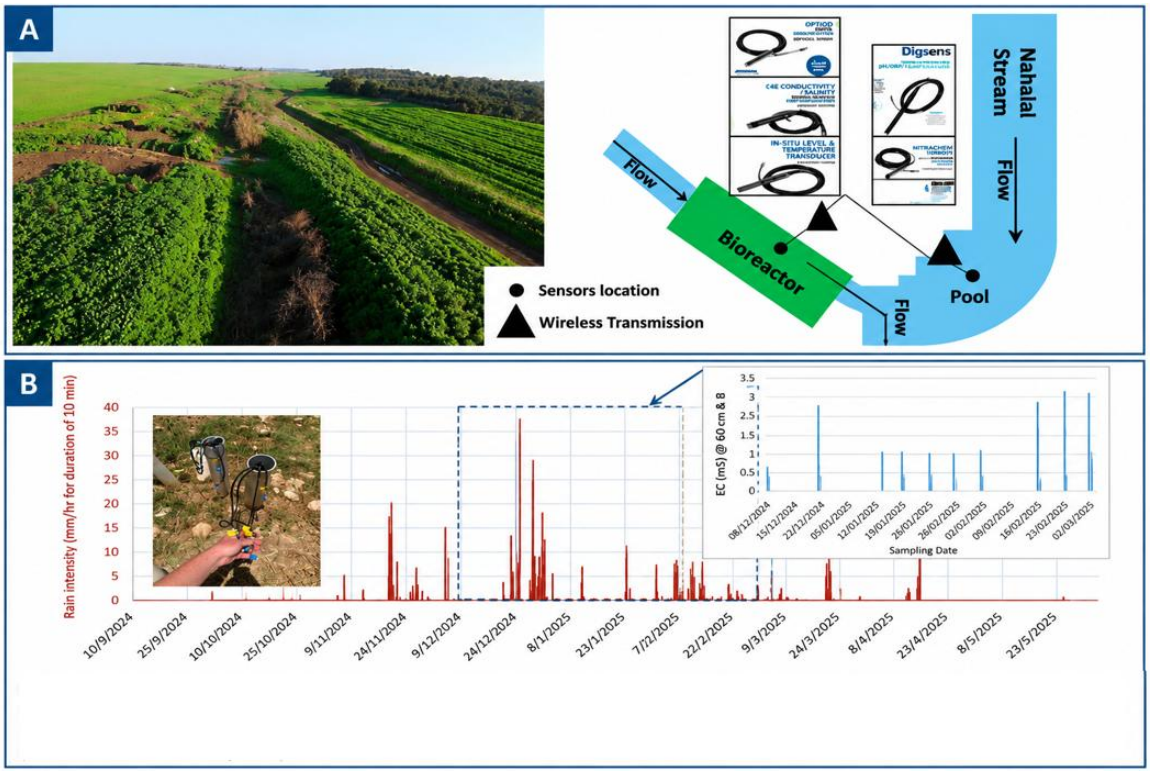


Figure 11. Monitoring setup and hydrological conditions of the Israeli bioreactor (BR). (A) Location of the BR within the drainage system and configuration of continuous sensors and wireless data transmission at the BR and downstream pool. (B) Rainfall intensity during the monitoring period and timing of grab-sampling events, with the inset showing electrical conductivity (EC) measurements at 60 cm depth at selected sampling dates.

3.4. Nitrogen removal performance

Total nitrogen (TN) was the main performance indicator for BR validation. Across the reported wet- and dry-period monitoring campaigns, mean TN concentration decreased from approximately 6 mg/L at the inlet to approximately 3 mg/L at the outlet, corresponding to an average reduction of about 50%. The spatial pattern in figure 12 supports the interpretation that N removal occurred within the reactive zone rather than only reflecting differences between separate inlet and outlet samples. Additional parameters—including pH, EC, phosphorus, calcium, potassium, TOC and heavy metals—were also measured.

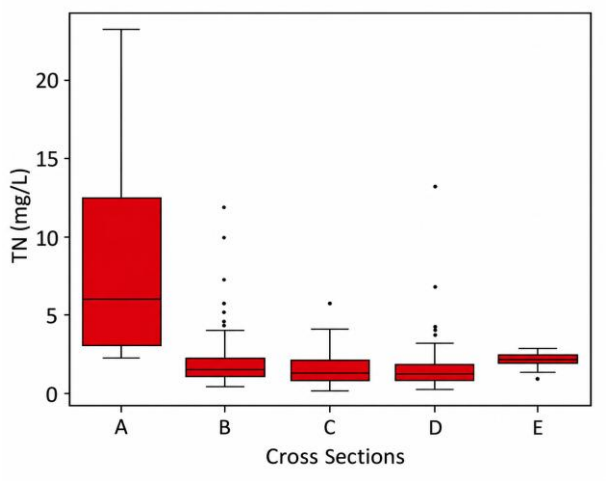


Figure 12. BR monitoring results for TN along the treatment path.

3.5. Hydrological context and groundwater monitoring

Because BR performance depends on water availability and hydraulic conditions, the reactor was evaluated within the wider hydrological monitoring network of the case-study site. Groundwater level and EC were monitored at selected piezometers, providing context for seasonal drainage conditions and for interpretation of BR operation. Figure 13 is used as supporting site context rather than as evidence of a direct BR effect on groundwater. It shows that the reactor operates within a dynamic hydrological setting, reinforcing the need to interpret treatment measurements together with rainfall, drainage and seasonal water-table conditions.

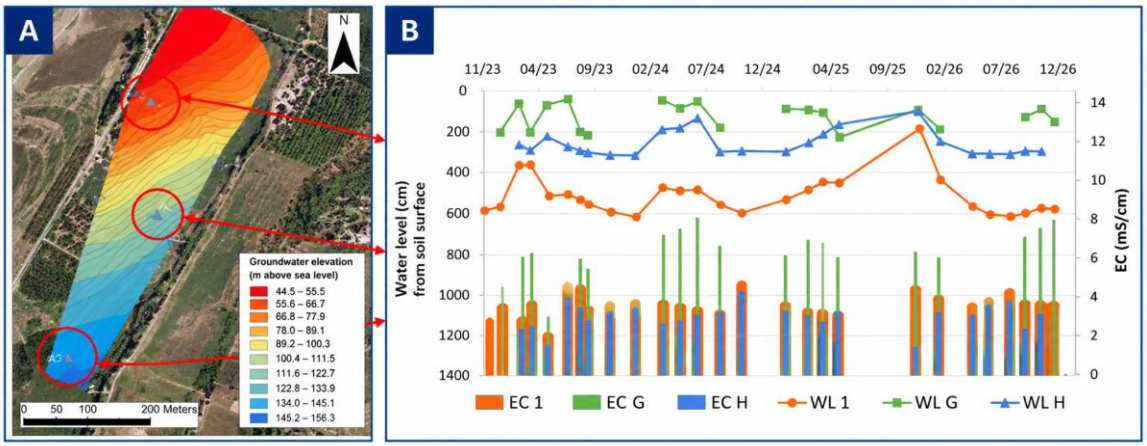


Figure 13. Groundwater conditions at the Israeli case-study site. (A) Spatial interpolation of groundwater elevation across the monitored area, showing the locations of selected piezometers. (B) Temporal variation in groundwater level (WL) and electrical conductivity (EC) measured at the selected monitoring locations.

3.6. Greenhouse gas investigation

A dedicated experiment was added to examine a potential environmental trade-off of denitrification (figure 14). Because nitrous oxide (N_2O) can be produced as an intermediate during microbial nitrogen transformations, samples were collected along the BR treatment path and transferred for headspace/spectroscopic analysis.

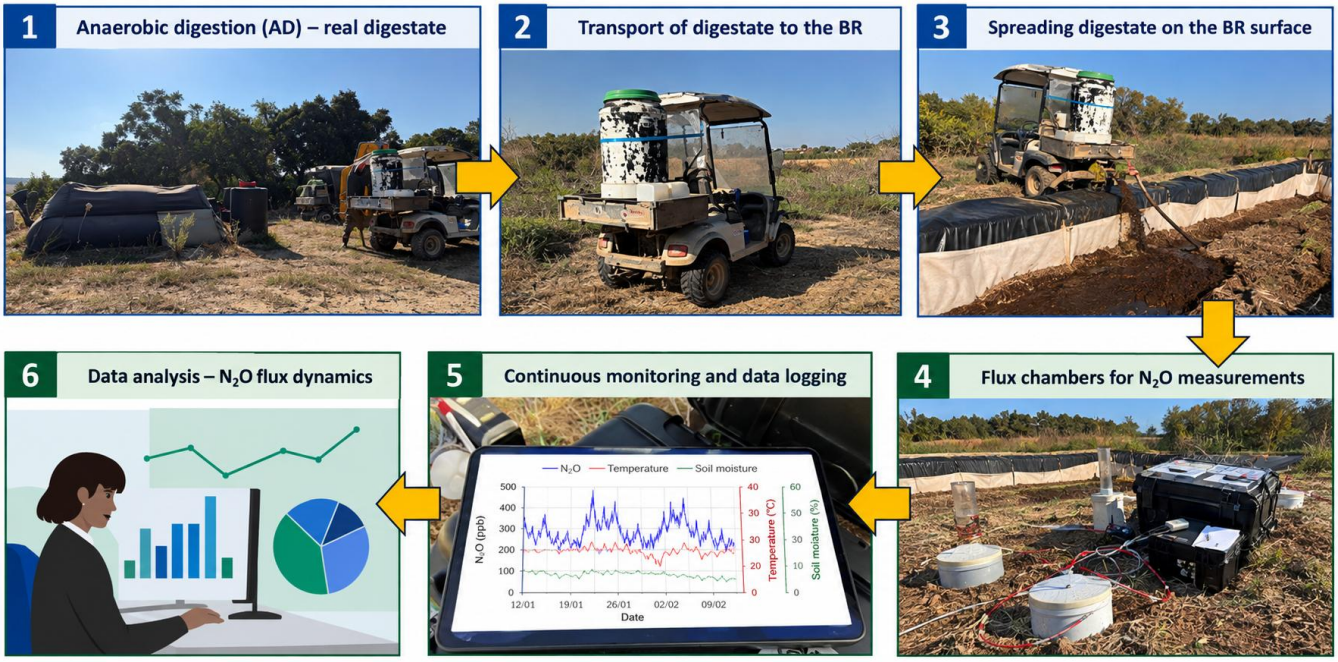
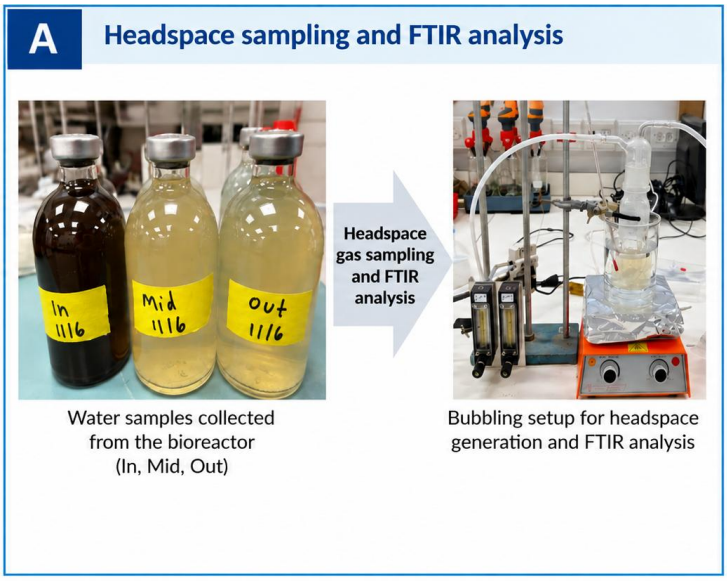


Figure 14. Experimental setup for monitoring N_2O dynamics following digestate application to the bioreactor (BR). Digestate produced by the anaerobic digestion (AD) system was transported to the BR and applied to its surface. N_2O dynamics were subsequently monitored using flux chambers installed along the BR, with continuous gas measurements and data logging used to characterize the temporal response following digestate application.

Surface flux measurements alone cannot determine whether the absence or reduction of an N_2O flux reflects limited N_2O formation within the reactor, retention/dissolution in the aqueous phase, or further microbial transformation before emission. Therefore, a complementary headspace analysis of water samples collected along the BR flow path (In, Mid, and Out) was performed. This analysis provided information on dissolved/volatile nitrogen species (N_2O and NH_3) within the reactor and enabled evaluation of their evolution during treatment. Combining the two approaches provides a more comprehensive assessment of potential gaseous nitrogen losses: flux chambers characterize actual surface emissions, whereas headspace analysis helps identify changes occurring within the aqueous phase along the treatment pathway. The headspace analysis results indicate substantial changes in nitrogen species during passage through the BR (figure 15). Dissolved N_2O was detected at the inlet (1.9 ± 0.5 µg L^{-1}) but was below detection at both the Mid and Out sampling locations, indicating no detectable accumulation of dissolved N_2O within the BR under the tested conditions. NH_3 showed a similarly pronounced decrease, from 13.4 mg L^{-1} at the inlet to 0.6 mg L^{-1} at Mid and 0.5 mg L^{-1} at the outlet. Together, these preliminary results suggest that nitrogen removal within the BR was not accompanied by accumulation of N_2O or NH_3 in the treated water. However, these measurements

represent dissolved/headspace-derived concentrations from a single experimental campaign and should not be interpreted as direct measurements of gaseous emissions or emission fluxes.



B Average N_2O and NH_3 concentrations in water samples

Sample location	N_2O ($\mu g\ L^{-1}$) Average ± SD	NH_3 ($mg\ L^{-1}$) Average ± SD
In	1.85 ± 0.50	13.43 ± 0.00
Mid	ND	0.63 ± 0.00
Out	ND	0.50 ± 0.00

Notes:
1. N_2O concentrations were calculated from measured headspace slopes and converted to $\mu g\ L^{-1}$ using a conversion factor of 1 $\mu mol\ L^{-1}$ = 44 $\mu g\ L^{-1}$.
2. Negative calculated N_2O values (Mid and Out) were below the detection limit and are reported as ND (not detected).
3. NH_3 concentrations were determined from FTIR absorbance in the 931 and 965 cm^{-1} region and reported in $mg\ L^{-1}$.

Figure 15. N_2O and NH_3 analysis of water samples collected along the bioreactor (BR). (A) Water samples collected at the BR inlet (In), middle section (Mid), and outlet (Out) were subjected to headspace generation by bubbling followed by gas analysis. (B) Average N_2O and NH_3 concentrations measured in the samples.

3.7. Main outcomes and relevance to D3.1

The Israeli case study demonstrates the progression of the denitrifying bioreactor (BR) from field-scale construction and adaptation to systematic validation under Mediterranean conditions. Following construction, the BR was modified in response to storm-related erosion and subsequently operated under contrasting seasonal conditions, including rainfall/runoff events during the wet season and controlled treated-wastewater application during the dry season. The monitoring strategy combined continuous environmental sensing with spatially and vertically resolved water sampling, allowing treatment performance to be evaluated along the BR flow path and under variable hydrological conditions.

The main validation results demonstrate effective nitrogen attenuation within the BR. Across the monitoring dataset, mean total nitrogen (TN) decreased from approximately 6 mg L^{-1} at the inlet to 3 mg L^{-1} at the outlet, corresponding to an average reduction of approximately 50%. Additional experiments were conducted to assess whether nitrogen removal could be associated with unintended gaseous nitrogen losses, particularly N_2O. Flux-chamber measurements were therefore complemented by headspace analysis of water samples collected at the inlet, middle, and outlet of the BR, providing information on both surface emissions and nitrogen species within the aqueous phase. In the headspace experiment, dissolved N_2O was detected at the inlet (1.9 ± 0.5 $\mu g\ L^{-1}$) but was not detected at the middle or outlet, while NH_3 decreased from 13.4 mg L^{-1} at the inlet to 0.6 and 0.5 mg L^{-1} at the middle and outlet, respectively. These results provide preliminary evidence that nitrogen attenuation within the BR was not accompanied by accumulation of N_2O or NH_3 in the treated water, while the flux-chamber measurements provide the complementary assessment of direct surface emissions.

Overall, the Israeli activity contributes to D3.1 by demonstrating field-scale BR operation and validation under realistic agricultural and climatic conditions, while extending the assessment beyond conventional water-quality performance to include potential gaseous nitrogen losses. The combined evaluation of TN removal, hydrological conditions, surface N_2O fluxes, and dissolved/headspace-derived nitrogen species provides a more comprehensive basis for assessing the environmental performance of the BR and identifying potential trade-offs associated with denitrification.

References

Coppola, A., Basile, A., Comegna, A. *et al.* FLOWS: a model to simulate water and solutes fluxes in agricultural and environmental systems: 2. Modules for specific applications in water and nutrient management. *Engineering with Computers* **42**, 194 (2026). https://doi.org/10.1007/s00366-026-02433-y

Coppola, A., Basile, A., Comegna, A. *et al.* FLOWS: a model to simulate water and solutes fluxes in agricultural and environmental systems. 1. Theory and applications with intercode benchmarking. *Engineering with Computers* (2026). [Accepted – In Press]. https://doi.org/ 10.1007/s00366-026-02428-9

Coppola, A., Comegna, A., and Hassan, S. B. M. (2026). Report on designing Drainage System and BR. The Italian and Israeli case studies. NPP-SOL Deliverable D2.1, PRIMA Section 2-2022. https://npp-sol.iamm.ciheam.org/wp-content/uploads/2025/02/D2-1-FINAL.pdf

Coppola, A., Zucaro, R., Baralla, S., Satta, M., Ruberto, M., Comegna, A., Dragonetti, G., & Hassan, S. B. M. (2024). Monitoring and Modelling Fluxes of Water and Nutrients to Surface Drainage Network from Irrigated Agricultural Fields in a Hydraulically Reclaimed Coastal Area. *Ecohydrology*, *17*(8), e2723. https://doi.org/https://doi.org/10.1002/eco.2723

Ghane, E., Fausey, N. R., and Brown, L. C. (2014). Non-Darcy flow of water through woodchip media. Journal of Hydrology, 519, 3400–3409. https://doi.org/10.1016/j.jhydrol.2014.09.065

Ghane, E., Fausey, N. R., and Brown, L. C. (2015). Modeling nitrate removal in a denitrification bed. Water Research, 71, 294–305. https://doi.org/10.1016/j.watres.2014.10.039

Hassan, S.B.M., Zuddas, G.L., Trudu, E., Comegna, A., Da Pelo, S., Lobina, F., Sessini, A.M., Coppola, A. (2026). Coupled agrohydrological and kinematic-wave modelling for agricultural bioreactor design. Ecohydrology. [Submitted]

Hoover, N. L., Bhandari, A., Soupir, M. L., and Moorman, T. B. (2016). Woodchip denitrification bioreactors: Impact of temperature and hydraulic retention time on nitrate removal. Journal of Environmental Quality, 45(3), 803–812. https://doi.org/10.2134/jeq2015.03.0161

Maxwell, B. M., Birgand, F., Schipper, L. A., Barkle, G., Rivas, A. A., Helmers, M. J., and Christianson, L. E. (2020). High-frequency, in situ sampling of field woodchip bioreactors reveals sources of sampling error and hydraulic inefficiencies. Journal of Environmental Management, 272, 110996. https://doi.org/10.1016/j.jenvman.2020.110996

Schipper, L. A., Robertson, W. D., Gold, A. J., Jaynes, D. B., and Cameron, S. C. (2010). Denitrifying bioreactors—An approach for reducing nitrate loads to receiving waters. Ecological Engineering, 36(11), 1532–1543. https://doi.org/10.1016/j.ecoleng.2010.04.008